High Throughput Optical Switching in Telecommunication Band via Hybrid Phase Change Metasurfaces

Amin Zamani, Gabriel Sanderson, Lu Zhang, Qiwei Miao, Sara Moujdi, Ze Zheng, Mohammadhossein Momtazpour, Christopher J. Mellor, Wending Zhang, Ting Mei, Zakaria Mansouri, Lei Xu, Mohsen Rahmani**

A. Zamani, G. Sanderson, S. Moujdi, Z. Zheng, M. Momtazpour, Z. Mansouri, C. Ying, L. Xu, M. Rahmani
Department of Engineering, School of Science and Technology, Nottingham Trent University, NG11 8NS, Nottingham, UK
Email Addresses: lei.xu@ntu.ac.uk and mohsen.rahmani@ntu.ac.uk

L. Zhang, Q. Miao, W. Zhang, Ting Mei
Key Laboratory of Light Field Manipulation and Information Acquisition, Ministry of Industry and Information Technology, School of Physical Science and Technology, Northwestern Polytechnical University, 710129, Xi'an, China

C. J. Mellor
School of Physics and Astronomy, Faculty of Science, University of Nottingham, NG7 2RD, Nottingham, UK

Funding:

Keywords: tunable metasurfaces, optical switching, phase change materials, laser tuning, Mie resonances

((**Abstract text.** The growing demand for more efficient data transmission has made nanoscale high-throughput all-optical switching a critical requirement in modern telecommunication systems. Metasurface-based platforms offer unique advantages because of their compact design, energy efficiency, and the ability to precisely manipulate light at the subwavelength scale, in a contact-less fashion. However, achieving both high transmission modulation and low optical loss in the telecom band remains a challenge. This study develops monolithic and hybrid metasurfaces based on the phase change material antimony trisulfide (Sb_2S_3) to address this limitation. First, we demonstrate the capability of Sb_2S_3 to offer up to ~91% modulation, even with a magnetic dipole – a low-Q resonance. It lifts the requirement for complex precisely fabricated metasurfaces, a long-standing limitation in the community for all optical switching. Furthermore, with the most straightforward hybridisation approach, i.e. depositing a thin film of silicon, we improved the simulated modulation depth to 99%. Experimentally, over 80% modulation was achieved for both hybrid and monolithic structures, with nearly 2-fold less power required for switching in the hybrid design whilst maintaining high modulation depth. This performance results from the significant refractive index tunability of Sb_2S_3 and its intrinsically low optical loss ($k<10^{-4}$) in the telecom band, further enhanced by silicon integration. The demonstrated metasurfaces offer an effective and scalable approach for all-optical light modulation with strong potential for integration into CMOS compatible photonic circuits and next-generation telecommunications systems.))

1. Introduction

Optical switching serves a fundamental role in telecommunication systems, enabling dynamic light modulation through switching, beam steering and wavefront control.[1-4] The rapid progress of nanofabrication in recent years has pushed all-optical switching into a new regime with compact, high-efficiency photonic devices, where their functionality and performance is increasingly governed by light-matter interactions at the nanoscale.[5,6] Building on these advances, metasurfaces—planar arrays of subwavelength resonant nanostructures—have emerged as powerful tools for manipulating the phase, amplitude, polarisation, and propagation direction of light by resonantly interacting with its electric and magnetic fields.[7,8] Among them, dielectric metasurfaces attract growing attention as they exhibit much lower optical losses in the infrared (IR) regions compared to their plasmonic counterparts,[9-12] and allow dynamic control through various switching mechanisms.[13-16]

In the recent years, enabling refractive index modulation through mechanical,[17], thermal,[15] thermoelectric,[14,18-20], electro-optic,[10] magnetic,[21] and laser-induced methods,[22] metasurfaces provide a dynamic platform for reconfigurable photonic applications.[23] However, the need for low-loss and high-contrast optical switching has revealed significant limitations in conventional tuning approaches. Thermal heaters need a continuous power supply to maintain refractive index changes, resulting in high static power consumption.[24] In the case of micro-electromechanical systems (MEMS), tuning is enabled through physical movement, but the approach involves complex fabrication and precise alignment. [25] Plasmonic metasurfaces, while capable of subwavelength confinement, suffer from significant ohmic losses, limiting their practical applications in telecommunication photonic systems.[9,11] Magnetic tuning methods can deliver continuous tuning of spectral resonances by smooth orientation of the magnetic field, but the approach is restricted by slow response, and limited pixel control.[21] In contrast, laser-tunable phase change materials (PCMs) have emerged as ideal candidates for low- loss tunable metasurfaces.[26,27]

Among the commonly explored PCMs such as $Ge_2Sb_2Te_5$ (GST),[15,28–32] $Ge_2Sb_2Se_4Te_1$ (GSST),[33] vanadium dioxide (VO_2),[16,19,34,35] Sb_2Se_3,[36-38] and Sb_2S_3,[37,39-44] the latter two have gained increasing interest in optics and photonics due to their low optical loss in the visible and IR ranges, large refractive index contrast between amorphous and crystalline phases, and compatibility with CMOS platforms. GST-based metasurfaces suffer from increased absorption after crystallisation and hence a reduction in optical efficiency.[30,32] Similarly, VO_2 metasurfaces demonstrate limited switching speed, and require continuous voltage to maintain thermal and switching stability.[16,35] As a result, Sb_2S_3 and Sb_2Se_3 have recently attracted a significant attention for the development of low-loss integrated photonic devices. While these metasurfaces show promise in optical switching,[45-49] current designs are limited by thermal actuation constraints, polarisation dependencies, and the need for complex dual-drive configurations to achieve balanced performance.[38,39,45]

In this work, we designed and fabricated Sb_2S_3/Si hybrid metasurfaces to enable high-throughput switching in telecommunication applications. To this end, an array of amorphous Sb_2S_3 metasurface pillars supporting a magnetic dipole resonance was fabricated and then selectively crystallised using a 532 nm laser under controlled conditions to achieve precise degree of crystallisation. Through the optimisation of pillar geometry and periodicity followed by detailed simulation and experimental transmission measurements, we show that by leveraging the large 0.74 refractive index change offered by the phase transition of Sb_2S_3, metasurface resonances can be tuned resulting in 91% transition modulation. To further improve the modulation depth, we engineered a hybrid structure by depositing a silicon layer on top of the metasurface, chosen to enhance near-field confinement and boost the quality factor of the resonances in the telecom band. The engineered hybrid design showed a potential for modulation depth of 99%, while requiring lower crystallisation laser power compared to the monolithic structure. Performance was experimentally evaluated through transmission measurements comparing the amorphous and polycrystalline hybrid and monolithic structures, validating our design approach and demonstrating the effectiveness of the hybrid configuration. Our findings underscore the potential of hybrid Sb_2S_3/Si metasurfaces for the development of high throughput optical switches.

2. Results and Discussion

2.1. Metasurface Characteristics

To demonstrate the versatility of Sb_2S_3 -based metasurface for optical switch, we first design a Sb_2S_3 metasurface consisting of periodically arranged Sb_2S_3 nanopillars supporting the lowest-order Mie-type resonance – the magnetic dipole (MD) resonance.[50-52] Although the MD resonance can be supported by various dielectric nanostructures, its broad spectral bandwidth has always limited its exploration for switching applications. In this work, we chose this resonance to demonstrate the remarkable capability of Sb_2S_3 for all-optical switching via such a low-Q resonance. This demonstration offers high tolerance to fabrication imperfections and strong field confinement within the pillars, enhancing the light-matter interaction in Sb_2S_3. Also, we specifically targeted the telecommunication wavelength range, which is highly relevant for integrated photonics and optical communication technologies. The height and radius of Sb_2S_3 pillars are set to be 300 and 325 nm, respectively.

As shown in **Figure 1**a, the refractive indices of the Sb_2S_3 film and the silicon layer were measured over a broad spectral range using spectroscopic ellipsometry, revealing a contrast of approximately n = 0.74 between the amorphous and crystalline phases of Sb_2S_3 in the telecommunication band. This significant difference enables effective optical tunability through phase transition. Here, for simplicity, a linear interpolation between amorphous and crystalline states was used to estimate the refractive index for intermediate states of crystallisation (**Equation S1** in Supporting Information). Figure 1b presents both SEM and optical microscope images of the metasurface in its amorphous (a) and polycrystalline (p-c) phases. In the microscope image, the p-c regions appear with a darker tone, allowing a clear visual distinction between the amorphous and crystallised areas. Figure 1c presents the schematic design of the Sb_2S_3 metasurface in both its amorphous and polycrystalline states. The switching behavior, indicated by red arrows, demonstrates how the metasurface can modulate light transmission based on the material phase and allow the structure to transmit or block light at specific wavelengths depending on its crystalline state.

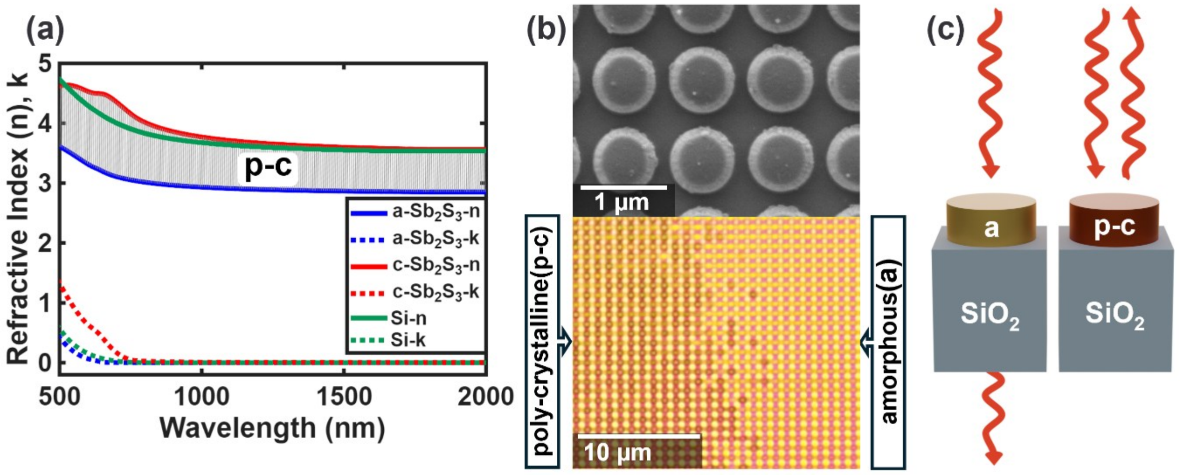

Figure 1. (a) Spectroscopic ellipsometry results of real and imaginary parts of the refractive indices of Sb_2S_3 (amorphous and crystalline phases) and silicon across the visible and infrared ranges, indicating the refractive index contrast of different phases of metasurface and the similarity of the refractive index of silicon and crystalline Sb_2S_3. The grey-shaded area indicates the polycrystalline phase of Sb_2S_3. (b) SEM and optical microscope images of the Sb_2S_3 metasurface. (c) Schematic of the monolithic PCM metasurface (radius: 325 nm, height: 300 nm, periodicity: 900 nm), illustrating transmission in the amorphous state and reflection in the polycrystalline state.

2.2. Optical Characterisation

Simulated transmission spectra of the PCM pillars for amorphous and polycrystalline cases are shown in **Figure 2**a. As can be seen, under the phase change of Sb_2S_3 from amorphous to polycrystalline state, we obtain a 140 nm resonance shift in simulation. This red shift arises from the increase in the refractive index, which lengthens the effective optical path in the nanostructures. By performing spherical multipolar analysis, the multipolar characteristics of the amorphous PCM metasurface are given in Figure 2b. The resonance near 1400 nm is primarily dominated by the excitation of the MD resonance as we designed, associated with some contributions from an electric dipole excitation (ED), electric quadrupole (EQ), and magnetic quadrupole (MQ) modes. Consequently, strong electric near-field confinement is observed within the PCM nanodisks, manifested by a circular-induced electric current (see **Figure S1**a field distribution in Supporting Information). As mentioned earlier, the MD offers relatively good field confinement and a broad resonance width, enabling effective control of the transmission response. The relatively low-Q nature of the MD mode facilitates broadband spectral switching in the infrared, while its localisation within the dielectric pillars causes high sensitivity of the central wavelength with respect to permittivity variations, as described by first order perturbation theory. As a result, we obtained a substantial resonance shift when the PCM is tuned from amorphous to polycrystalline state.

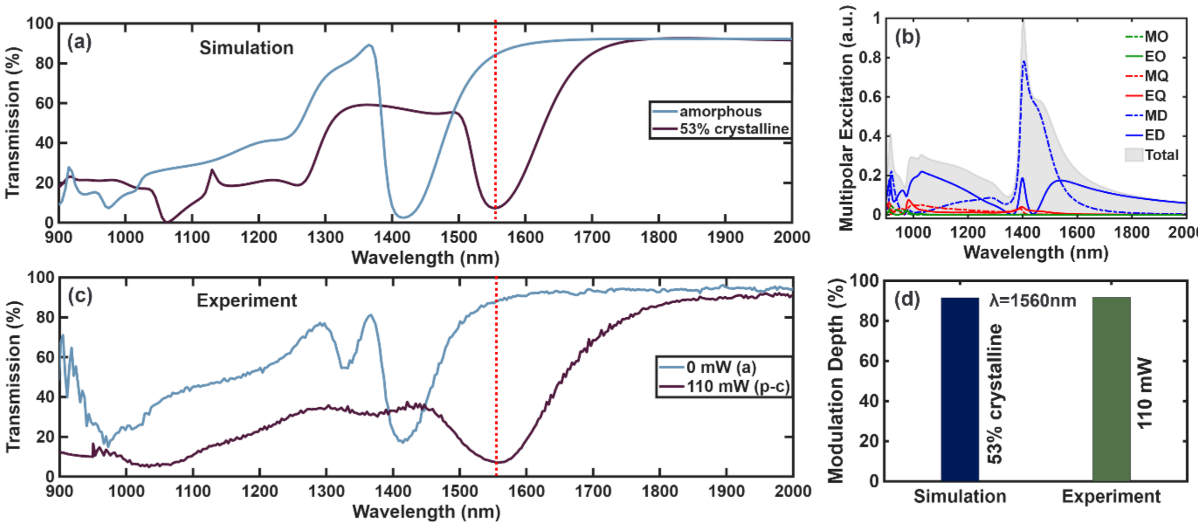

Figure 2. (a) Simulated transmission spectra of the PCM metasurface showing a 140 nm redshift with a transmission reduction at 1560 nm indicated by the dashed red line. (b) Multipole decomposition at 1560 nm indicating dominant magnetic dipole contributions. (c) Experimental transmission spectra validating simulations, with resonances near 1300 and 1400 nm in amorphous and 1560 nm in polycrystalline structure. (d) Simulated and experimental modulation depth of 91.5% and 92% at 1560 nm, respectively.

Experimentally, the phase transition was induced using a continuous-wave (CW) CNI laser at 532 nm, focused onto the metasurface, optically crystallising the Sb_2S_3. Experimental transmission measurements were performed using the setup shown in Supporting Information **Figure S2**. The measured transmission spectra of the monolithic structure, shown in Figure 2c, validate the simulations by showing the resonance 1400 nm in the amorphous phase, and a redshifted resonance near 1560 nm in the polycrystalline phase. As a result, using the broadband MD resonance with the Sb_2S_3 nanopillar metasurface, we experimentally achieved an optically induced transmission modulation depth of up to ~92% (Figure 2d), demonstrating the strong potential of Sb_2S_3 based metasurface for high-performance optical switching applications. Simulations suggest that achieving this switching functionality requires approximately 53% crystallisation of the PCM. Experimental switching to the opaque state is accomplished by applying a laser power of 110 mW. The corresponding laser irradiance is described by

$$I(r) = \frac{2P}{\pi\omega_0^2}\exp\left(-\frac{2r^2}{\omega_0^2}\right) \quad (1)$$

where ω_0 is the beam waist, r is the radial distance from the beam center, and P is the laser power, assuming a Gaussian beam profile. Under 110 mW power with a 100 μm beam radius, the corresponding switching energy per square centimetre i.e. the energy density in the monolithic structure was calculated to be 7 $kJcm^{-2}$. The initial crystallisation threshold energy density was also calculated based on Equation 1 as $E_0 = I(r=0) \times t = 3.8$ $kJcm^{-2}$ at the beam centre, using $P_0 = 60$ mW laser power, 10 μm beam radius, and an exposure time of $t = 100$ ms. These values establish the operational threshold energy required to initiate crystallisation in the PCM and define the practical energy conditions for driving the transition between the transmissive and opaque states.

As has been shown, owing to the large refractive index changes of the Sb_2S_3, the designed MD-based PCM metasurface demonstrates high optical transmission switching under optical excitation. In addition, our designed PCM metasurface suggests promising potential for integration into high-numerical aperture (NA) optical systems. **Figure S3**(a–d) in the Supporting Information shows that the monolithic metasurface maintains large incident-angle independency across the infrared range, with high transmission and minimal angular dependence up to 50° at 1314 nm and 1422 nm for the half- and fully crystalline states.

To further demonstrate the versatility of the Sb_2S_3-based metasurface platform for optical switching, we integrated Sb_2S_3 with silicon to create a hybrid metasurface. Silicon was specifically chosen for its high refractive index, which provides strong contrast with amorphous Sb_2S_3 while closely matching the crystalline phase enabling enhanced near-field confinement control. The hybrid platform provides a stable optical response, and excellent compatibility with integrated photonic circuits, and large resonance tunability offered by Sb_2S_3. This combination offers a powerful route to enhance the dynamic control of light-matter interactions and expand the functionality of conventional silicon photonic devices. In the following, we design a hybrid Sb_2S_3/Si metasurface that supports high-Q resonances, enabling both enhanced near-field confinement and efficient far-field modulation.

Our designed hybrid Sb_2S_3/Si metasurface consists of a Sb_2S_3 nanodisk metasurface with 100-nm-thick silicon layer on top to enable optimal modulation depth in the telecom range (optimised through parametric simulations as shown in **Figure S4** in Supporting Information), as illustrated in **Figure 3**a. The deposition of a thin silicon layer modifies the transmission channels of nonresonant modes. Their interaction with the leaky channels of guided mode resonances, alters the overall spectral features, giving rise to narrow asymmetric lineshapes, characteristic of Fano-like intereference.[53-57] As can be seen from the simulated transmission spectra in Figure 3a, such a combination of Sb_2S_3 nanodisk metasurface with silicon layer can introduce high-Q resonances in the telecom spectral range. Notably, a pronounced resonance is formed around 1457 nm (Figure 3a), dominated by the EO, ED, and MQ excitation, as shown in Figure 3b. Accordingly, owing to the strong multipolar excitation, the induced electric near-field is highly confined within the PCM and silicon nanostructures (see Figure S1b of the electric near field distribution in the Supporting Information). The strong field enhancement at the interface between the PCM nanodisk and silicon layer causes the resonance to be highly sensitive to variations in the refractive index in both silicon and PCM, so that a slight change in the PCM's refractive index can result in a significant transmission conversion and 99% modulation depth, as demonstrated by Figure 3a inset. These properties suggest the potential of the hybrid metasurface for applications such as tunable metasurface modulators and nonlinear light sources with switchable emission characteristics.

Furthermore, we simulate the transmission spectra at different crystallisation stages, as shown in **Figure S5** in the Supporting Information, capturing the gradual and dynamic tunability of the system. These results suggests that such a hybrid Sb_2S_3/Si metasurface platform enables broadband, reconfigurable spectral control, reinforcing its promise as a versatile platform for tunable photonic components and all-optical switching applications.

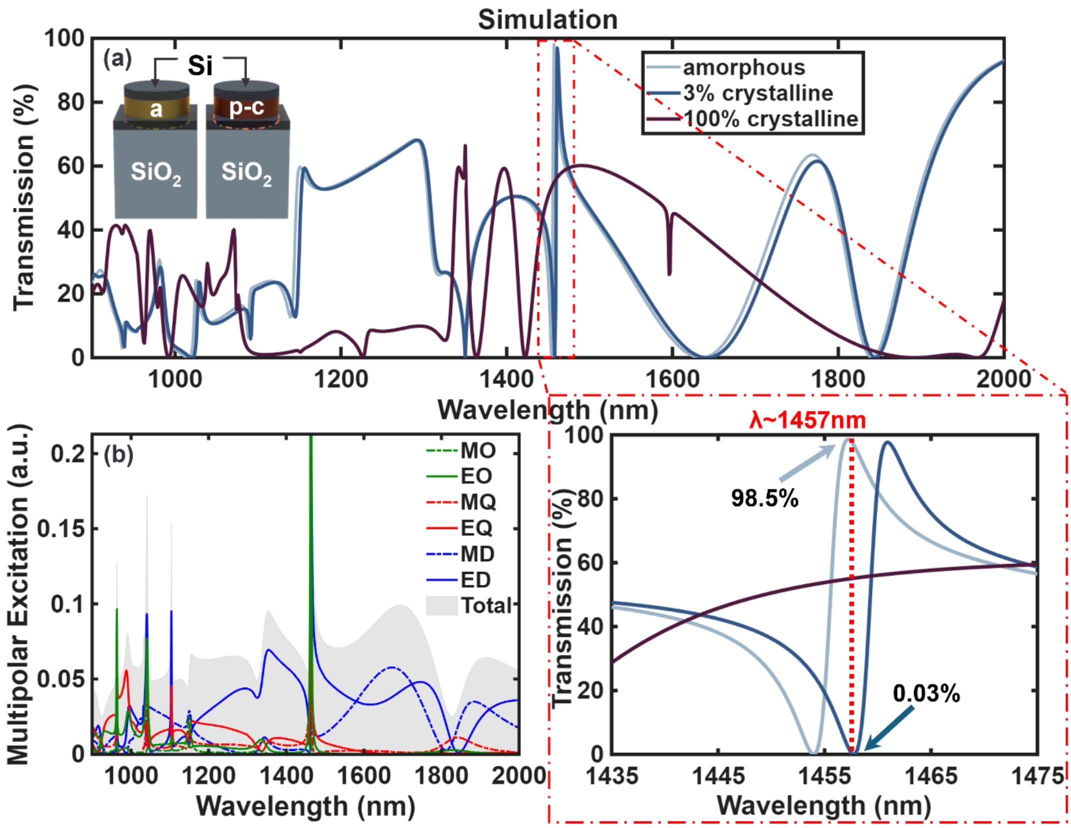

Figure 3. (a) Simulated transmission spectra of the hybrid structure in the amorphous state and under partial and full crystallisation, indicating sharp resonances in the infrared range. The schematic of the hybrid structure is also shown. Inset: Transmission conversion achieved with 3% crystallisation. (b) Multipole decomposition revealing dominant octupolar resonance contributions around 1457 nm.

To validate the simulation results, the Sb_2S_3/Si metasurface was exposed to green CW laser powers of 61 and 65 mW. The resulting transmission spectra in the infrared range, shown in **Figure 4**a, indicate a sharp resonance between 1400 and 1500 nm. Applying 65 mW, the transmission at 1450 nm was modulated by approximately 90%, confirming the switching functionality. In the hybrid configuration, the required switching energy was significantly lower, with effective modulation achieved in 100 ms at 65 mW using a 10 µm focus. This corresponds to a reduction in energy density from 7 $kJcm^{-2}$ to 4.1 $kJcm^{-2}$ (110 mW vs. 65 mW laser power, respectively), primarily because the hybrid structure requires only partial crystallisation of the PCM to shift the transmission from the transmissive to the opaque state. Although a minimum power is necessary to initiate crystallisation, the hybrid design inherently enables switching at lower power levels, further helped by the silicon layer's insulation effect, which raises the Sb_2S_3 temperature and lowers the threshold for phase change.

Although factors such as approximations in silicon deposition modelling and the limited resolution of the spectrometer affect the accuracy of the measurements, the hybrid metasurface still exhibits a pronounced resonance experimentally. It is worth noting that even with the fabrication imperfections, the structure maintains strong resonant feature and demonstrates significant light modulation, indicating the robustness and practical potential of the hybrid design.

To assess the effect of laser power on the silicon layer, we measured the transmission spectrum of a 100-nm-thick silicon film on SiO_2 substrate under input pump powers ranging from 61 mW to 65 mW (Figure 4b). As can be seen, the transmission spectrum of the silicon layer remains stable, indicating that the optical properties of silicon are unchanged under the applied laser powers. In contrast, when integrated with Sb_2S_3, the hybrid metasurface exhibits a pronounced transmission conversion, varying from 88% to 8% with only a 4 mW increase in input power, clearly demonstrating the strong tunability enabled by the Sb_2S_3 component. These results highlight the hybrid Sb_2S_3/Si metasurface as a highly efficient and low-loss platform for optical switching. The combination of different materials not only provides a new route for constructing strong resonance that can boosting light-matter interactions within both media, but also leverages their complementary advantages, for example, enabling broadband, highly tunable nonlinear silicon meta-devices driven by the Sb_2S_3. Moreover, the ability to combine the stability of silicon with the dynamic tunability of Sb_2S_3 opens new opportunities for reconfigurable photonic devices, adaptive optical components, and integrated light–matter interaction control.

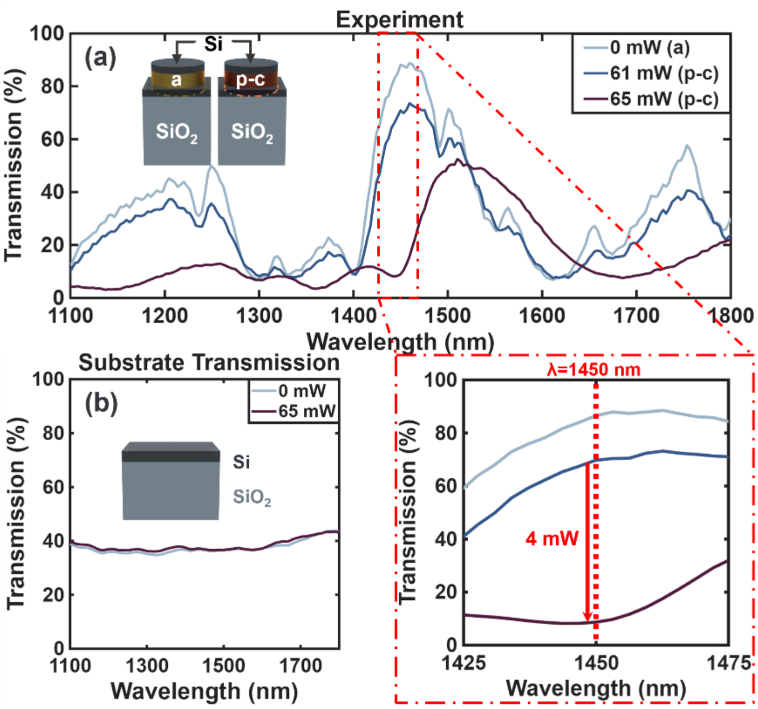

Figure 4. (a) Experimental transmission spectra of the Sb_2S_3/Si hybrid metasurface under laser powers of 0, 61 and 65 mW, showing a clear transmission drop at 1450 nm due to crystallisation.

Inset: zoomed view of the transmission conversion. (b) Transmission of the silicon substrate before and after laser exposure.

Table 1 presents a comparison of typical metasurface-based optical switches from the literature with our device. The optical modulation depth η -the percentage change between maximum and minimum transmission relative to absolute maximum transmission- for monolithic and hybrid structures is calculated using the equation provided, with results based on Figure 2–Figure 4 summarised in Table 1. Our device demonstrates the potential for a large modulation depth of 91%, because of the tunability and low-loss properties of Sb_2S_3. In the hybrid structure, the ability to reach nearly 99% modulation depth is shown through simulation by incorporating a silicon layer, which enhances optical confinement. The highest modulation depth occurs at 1457 nm with only 3% crystallisation, highlighting the capability of the hybrid design for efficient, low-energy, high-contrast optical switching.

Table 1: Comparison of several optical switches

Method	Contrast Ratio[39]/ Modulation depth	Switching Speed	Direction	Stimulus	Demonstrated Wavelength
Sb_2S_3 [39]	CR[a)] = 22 dB	35 minutes	Reflection	Annealing inside a heating cell	1045 and 1080 nm
Sb_2S_3 [40]	54% to 18% η = 66.7%	-	Reflection	-	550nm
Sb_2S_3 and Sb_2Se_3 [36]	20% to 10% η = 50%	400 ns a[b)] 100 ms c[c)]	Reflection	Annealing on hot plate or 638nm pulsed diode laser	1550nm
GSST[d)] [33]	9% to 31% η ~ 70% CR= 42 dB	100 ns a 100 ms c	Reflection	Laser pulse and electrothermal joule heating	1560 to 1563 nm
Silicon [18]	η = 90%	10 ms	Transmission and Reflection	0 to 5 V electrically localised heating	740 and 780 nm
Silicon [13]	η = 60%	65 fs	Transmission	Ti: Sapphire laser at 780 nm, 45 fs duration	755-780 nm
GST[e)] [26]	η ~ 25% CR = 14.3 dB	100 ns a	Transmission	Optical pulses	1530-1565 nm
VO_2 [35]	CR = 20.8 dB	350 ms ON 771 ms OFF	Reflection	voltage-controlled Joule heating generated by laser-induced graphene	1648 nm
This work	**M[f)]: η = 91%** **H[g)]: η = 99%**	**100 ms**	**Transmission**	**CW 532 nm laser**	**M: 1560 nm** **H: 1460 nm**

[a)]contrast ratio, [b)]amorphisation; [c)]crystallisation; [d)]Ge-Sb-Se-Te, [e)]$Ge_2Sb_2Te_5$, [f)]monolithic, [g)]hybrid

Modulation depth (η) is calculated using the Equation 2:

$$\eta = \left[\frac{T_{max} - T_{min}}{T_{absolute\ max}}\right] \times 100 \qquad (2)$$

where T_{max} and T_{min} are the maximum and minimum transmission intensities, and $T_{absolute\ max}$ is the highest absolute transmission.

3. Conclusions

We have designed and fabricated a hybrid optical switch based on Sb_2S_3 and silicon metasurfaces operating at telecommunication wavelengths. Switching was successfully achieved using a CW laser at 532 nm. We demonstrated that the hybrid structure requires significantly less power and demonstrates higher switching efficiency compared to that of the monolithic design, defined here as the modulation depth between the ON and OFF states. Our design enables up to 99% modulation depth through partial crystallisation, offering a versatile way to control light transmission. the demonstrated switching behavior in the hybrid structure marks a significant step toward efficient, reconfigurable optical devices for telecom applications.

4. Experimental Section

4.1. Metasurface Fabrication

Sb_2S_3 nanopillars were fabricated through standard electron beam lithography and etching. The Sb_2S_3 film was deposited by thermal evaporation on a fused silica substrate. For hybridisation, an silicon layer was deposited using plasma-enhanced chemical vapour deposition (PECVD).

4.2. Optical Characterisation

Transmission measurements were performed using a Köhler illumination setup with a Thorlabs SLS302 white light source and an Ocean Optics NIRQuest spectrometer. Phase transitions were induced using a 2.5 W, 532 nm DPSS CW laser (CNI). Simulations were conducted using rigorous coupled-wave analysis (RCWA) in MATLAB and the finite element method in COMSOL Multiphysics.

Acknowledgements

This research work has been kindly supported by the Royal Society and the Wolfson Foundation. The authors appreciate the use of the NTU Imaging Suite, NTU High Performance Computing cluster Avicenna, and NTU Medical Technologies Innovation Facility (MTIF). G.S. acknowledges support from the Nottingham BBSRC.

Data Availability Statement

The data that support the findings of this study are available from the corresponding author upon reasonable request.

Supporting Information

Supporting Information is available from the author.

References

1. Bishop, D. J. Giles, C. R. and S. R. Das, “The Rise of Optical Switching,” *Scientific American* 284, no. 1 (2001): 88–94.
https://doi.org/10.1038/scientificamerican0101-882. Sasikala, V. and K. Chitra, “All Optical Switching and Associated Technologies: A Review,” *Journal of Optics* 47, no. 3 (2018): 307–317.
https://doi.org/10.1007/s12596-018-0452-3

3. X. Chen, J. Lin, and K. Wang, “A Review of Silicon‐Based Integrated Optical Switches,” *Laser & Photonics Reviews* 17, no. 4 (2023): 2200571.
https://doi.org/10.1002/lpor.202200571

4. K. Asakawa, Y. Sugimoto, and S. Nakamura, “Silicon photonics for telecom and data-com applications,” *Opto-Electronic Advances* 3, no. 10 (2020): 200011-1.
https://doi.org/10.29026/oea.2020.200011

5. Belotti, M. Galli, M. Gerace, D. Andreani, L. C. Guizzetti, G. Md Zain, A. R. Johnson, N. P. Sorel, M. and R. M. De La Rue, “All-Optical Switching in Silicon-on-Insulator Photonic Wire Nano–Cavities,” *Optics Express* 18, no. 2 (2010): 1450–1461.
https://doi.org/10.1364/OE.18.001450

6. Jiang, Xinpeng, Dingbo Chen, Zhaojian Zhang, Jie Huang, Kui Wen, Jie He, and Junbo Yang. "Dual-channel optical switch, refractive index sensor and slow light device based on a graphene metasurface." *Optics Express* 28, no. 23 (2020): 34079-34092.
https://doi.org/10.1364/OE.412442

7. N. Yu, P. Genevet, M. A. Kats, F. Aieta, J.-P. Tetienne, F. Capasso, and Z. Gaburro, “Light propagation with phase discontinuities: generalized laws of reflection and refraction,” *Science* 334, no. 6054 (2011): 333–337.
https://doi.org/10.1126/science.1210713

8. Lalanne, P. Astilean, S. Chavel, P. Cambril, E. Launois, H., “Blazed binary subwavelength gratings with efficiencies larger than those of conventional échelette gratings,” *Optics Letters* 23, no. 14 (1998): 1081–1083.
https://doi.org/10.1364/OL.23.001081

9. X. Zhang and J. Yang, “Ultrafast Plasmonic Optical Switching Structures and Devices,” *Frontiers in Physics* 7 (2019): 190.
https://doi.org/10.3389/fphy.2019.00190

10. Xie, Z. T. Wu, J. Fu, H. Y. and Q. Li, “Tunable Electro- and All-Optical Switch Based on Epsilon-Near-Zero Metasurface,” *IEEE Photonics Journal* 12, no. 4 (2020): 1–10.
https://doi.org/10.1109/JPHOT.2020.3010284

11. Wang, H. Hu, Z. Deng, J. Zhang, X. Chen, J. Li, K. and G. Li, “All-Optical Ultrafast Polarization Switching with Nonlinear Plasmonic Metasurfaces,” *Science Advances* 10, no. 8 (2024): eadk3882.
https://doi.org/10.1126/sciadv.adk3882

12. Im, S. Deng, Y. Bozhevolnyi, S. I. and F. Ding, “Spin-Controlled Generation of a Complete Polarization Set with Randomly-Interleaved Plasmonic Metasurfaces,” *Opto-Electronic Advances* 7, no. 8 (2024): 240076-1.
https://doi.org/10.29026/oea.2024.240076

13. M. R. Shcherbakov, P. P. Vabishchevich, A. S. Shorokhov, et al., “Ultrafast All-Optical Switching with Magnetic Resonances in Nonlinear Dielectric Nanostructures,” *Nano Letters* 15, no. 10 (2015): 6985–6990.
https://doi.org/10.1021/acs.nanolett.5b02989

14. M. Rahmani, L. Xu, A. E. Miroshnichenko, et al., “Reversible Thermal Tuning of All‐Dielectric Metasurfaces,” *Advanced Functional Materials* 27, no. 31 (2017): 1700580.
https://doi.org/10.1002/adfm.201700580

15. Choi, C. Lee, S.-Y. Mun, S.-E. Lee, G.-Y. Sung, J. Yun, H. Yang, J.-H. Kim, H.-O. Hwang, C.-Y. and B. Lee, “Metasurface with Nanostructured $Ge_2Sb_2Te_5$ as a Platform for Broadband-Operating Wavefront Switch,” *Advanced Optical Materials* 7, no. 12 (2019): 1900171.
https://doi.org/10.1002/adom.201900171

16. King, J. Wan, C. Park, T. J. Deshpande, S. Zhang, Z. Ramanathan, S. and M. A. Kats, “Electrically Tunable VO_2–Metal Metasurface for Mid-Infrared Switching, Limiting and Nonlinear Isolation,” *Nature Photonics* 18, no. 1 (2024): 74–80.
https://doi.org/10.1038/s41566-023-01324-8

17. Z. Guanxing, Z. Liu, W. Deng, and W. Zhu, "Reconfigurable Metasurfaces with Mechanical Actuations: Towards Flexible and Tunable Photonic Devices," *Journal of Optics* 23, no. 1 (2020): 013001.
https://doi.org/10.1088/2040-8986/abcc52

18. K. Zangeneh Kamali, L. Xu, N. Gagrani, et al., "Electrically Programmable Solid-State Metasurfaces via Flash Localised Heating," *Light: Science & Applications* 12, no. 1 (2023): 40.
https://doi.org/10.1038/s41377-023-01078-6

19. Wang, X. Wang, Q. Ren, H. Cai, J. Xin, Y. Lang, X. Xiao, Z. Lan, J. You, and W. E. I. Sha, "Temperature-Controlled Optical Switch Metasurface with Large Local Field Enhancement Based on FW-BIC," *Frontiers in Nanotechnology* 5 (2023): 1112100.
https://doi.org/10.3389/fnano.2023.1112100

20. Wang, Y. Landreman, P. Schoen, D. Okabe, K. Marshall, A. Celano, U. Wong, H.-S. P. Park, J. and M. L. Brongersma, "Electrical Tuning of Phase-Change Antennas and Metasurfaces," *Nature Nanotechnology* 16, no. 6 (2021): 667–672.
https://doi.org/10.1038/s41565-021-00882-8

21. Y. V. Izdebskaya, Z. Yang, M. Liu, et al., "Magnetic Tuning of Liquid Crystal Dielectric Metasurfaces," *Nanophotonics* 11, no. 17 (2022): 3895–3900.
https://doi.org/10.1515/nanoph-2022-0101

22. M. Alvarez‐Alegria, J. Siegel, M. Garcia‐Pardo et al., "Nanosecond Laser Switching of Phase‐Change Random Metasurfaces with Tunable ON‐State," *Advanced Optical Materials* 10, no. 3 (2022): 2101405.
https://doi.org/10.1002/adom.202101405

23. Li, H. Zou, X. Lu, C. Wang, and S.-S. Lee, "Polarization-Multiplexed Metasurface-Based Retroreflective and Specular Reflection Enabling High-Efficient Optical Switch," in *Proceedings of the 2024 IEEE Opto-Electronics and Communications Conference (OECC)* (2024): 1–3.
https://doi.org/10.1109/OECC54135.2024.10975347

24. A. Parveen, A. Irshad, D. Tyagi, M. Alam, A. Kazim, F. Ahmad, K. Tao, and Z. Ouyang, "Design and Optimization of a Thermally Tunable Vanadium Dioxide-Based Metasurface Optical Switch for Mid-Infrared Applications," Silicon (2025): 1–11.
https://doi.org/10.1007/s12633-025-03425-1

25. Plander and M. Stepanovsky, "MEMS technology in optical switching," in *Proceedings of the 2017 IEEE 14th International Scientific Conference on Informatics* (2017): 299–305. https://doi.org/10.1109/INFORMATICS.2017.8327264

26. J. Von Keitz, J. Feldmann, N. Gruhler, et al., "Reconfigurable Nanophotonic Cavities with Nonvolatile Response," *ACS Photonics* 5, no. 11 (2018): 4644–4649. https://doi.org/10.1021/acsphotonics.8b01127

27. M. Wuttig, H. Bhaskaran, and T. Taubner, "Phase-Change Materials for Non-Volatile Photonic Applications," *Nature Photonics* 11, no. 8 (2017): 465–476. https://doi.org/10.1038/nphoton.2017.126

28. C. Zhang, M. Zhang, Y. Xie, et al., "Wavelength-Selective 2×2 Optical Switch Based on a $Ge_2Sb_2Te_5$-Assisted Microring," *Photonics Research* 8, no. 7 (2020): 1171–1176. https://doi.org/10.1364/PRJ.393513

29. H. Hu, H. Zhang, L. Zhou, et al., "Contra-Directional Switching Enabled by Si-GST Grating," *Optics Express* 28, no. 2 (2020): 1574–1584. https://doi.org/10.1364/OE.381502

30. Q. Zhu, S. Shi, J. Wang, Q. Fang, M. Li, and J. Dong, "Linear Optical Switch Metasurface Composed of Cross-Shaped Nano-Block and $Ge_2Sb_2Te_5$ Film," *Optics Communications* 498 (2021): 127222. https://doi.org/10.1016/j.optcom.2021.127222

31. S. Wredh, Y. Wang, J. K. W. Yang, and R. E. Simpson, "Multi‐Level Optical Switching by Amorphization in Single‐ and Multi‐Phase Change Material Structures," *Advanced Optical Materials* 12, no. 5 (2024): 2301835. https://doi.org/10.1002/adom.202301835

32. Zhang, Z. Yang, J. Bai, W. Han, Y. He, X. Huang, J. Chen, D. Xu, S. and W. Xie, "All-Optical Switch and Logic Gates Based on Hybrid Silicon-$Ge_2Sb_2Te_5$ Metasurfaces," *Applied Optics* 58, no. 27 (2019): 7392–7396. https://doi.org/10.1364/AO.58.007392

33. Y. Zhang, J. B. Chou, J. Li, et al., "Broadband Transparent Optical Phase Change Materials for High-Performance Nonvolatile Photonics," *Nature Communications* 10, no. 1 (2019): 4279. https://doi.org/10.1038/s41467-019-12196-4

34. K. J. Miller, K. A. Hallman, R. F. Haglund Jr., and S. M. Weiss, "Silicon Waveguide Optical Switch with Embedded Phase Change Material," *Optics Express* 25, no. 22 (2017): 26527–26536.
https://doi.org/10.1364/OE.25.026527
35. Y. Ma, H. Zhou, Y. Huang, et al., "Electrically Controllable Optical Switch Metasurface Based on Vanadium Dioxide," *Optics Letters* 48, no. 15 (2023): 3885–3888.
https://doi.org/10.1364/OL.492350
36. M. Delaney, I. Zeimpekis, D. Lawson, D. W. Hewak, and O. L. Muskens, "A New Family of Ultralow Loss Reversible Phase‐Change Materials for Photonic Integrated Circuits: Sb_2S_3 and Sb_2S_3," *Advanced Functional Materials* 30, no. 36 (2020): 2002447.
https://doi.org/10.1002/adfm.202002447
37. O. Hemmatyar, S. Abdollahramezani, I. Zeimpekis, et al., "Enhanced Meta-Displays Using Advanced Phase-Change Materials," *arXiv* arXiv:2107.12159 (2021).
38. X. Yang, L. Lu, Y. Li, et al.,"Non‐Volatile Optical Switch Element Enabled by Low‐Loss Phase Change Material," *Advanced Functional Materials* 33, no. 42 (2023): 2304601.
https://doi.org/10.1002/adfm.202304601
39. D. Pérez-Francés, G. Santos, J. Resl, M. Losurdo, Y. Gutiérrez, and F. Moreno, "Sb_2S_3-Based Optical Switch Exploiting the Brewster Angle Phenomenon," *Optical Materials Express* 13, no. 12 (2023): 3677–3687.
https://doi.org/10.1364/OME.502327
40. H. Li, B. Long, T. Wang, F. Zhou, Y. Xu, and Z. Zhang, "Visible Metasurface Using an Sb_2S_3 Nanodisk Structure for Stretchable Color Application," *Optics Communications* 554 (2024): 130205.
https://doi.org/10.1016/j.optcom.2023.130205
41. T. Liu, D. Zhang, W. Liu, et al., "Phase-Change Nonlocal Metasurfaces for Dynamic Wavefront Manipulation," *Physical Review Applied* 21, no. 4 (2024): 044004.
https://doi.org/10.1103/PhysRevApplied.21.044004
42. K. Liu, Z. Lin, B. Han, M. Hong, and T. Cao, "Non-volatile dynamically switchable color display via chalcogenide stepwise cavity resonators," *Opto-Electronic Advances* 7, no. 1 (2024): 230033-1.
https://doi.org/10.29026/oea.2024.230033

43. Zhang, L. Gao, K. Lu, F. Xu, L. Rahmani, M. Sun, L. Gao, F. Zhang, W. and T. Mei, "Visible-Band Chiroptical Meta-Devices with Phase-Change Adjusted Optical Chirality," *Nano Letters* 22, no. 18 (2022): 7628–7635.
https://doi.org/10.1021/acs.nanolett.2c02739

44. Gao, K. Du, K. Tian, S. Wang, H. Zhang, L. Guo, Y. Luo, B. Zhang, W. and T. Mei, "Intermediate Phase-Change States with Improved Cycling Durability of Sb_2S_3 by Femtosecond Multi-Pulse Laser Irradiation," *Advanced Functional Materials* 31, no. 35 (2021): 2103327.
https://doi.org/10.1002/adfm.202103327

45. X. Yang, M. S. Nisar, W. Yuan, et al., "Phase Change Material Enabled 2×2 Silicon Nonvolatile Optical Switch," *Optics Letters* 46, no. 17 (2021): 4224–4227.
https://doi.org/10.1364/OL.435552

46. X. Chen, J. Lin, and K. Wang, "A Review of Integrated Photonic Devices Using Sb_2Se_3," *Advanced Physics Research* 4, no. 1 (2025): 2400080.
https://doi.org/10.1002/apxr.202400080

47. S. Gao, R. Haonan, P. Jingzhe, et al., "Reconfigurable Free Form Silicon Photonics by Phase Change Waveguides," *Advanced Optical Materials* 13, no. 15 (2025): 2402997.
https://doi.org/10.1002/adom.202402997

48. Q. Zhang, Q. Hong, and Z. Zhu, "Low-Loss Optical Switching Based on Phase-Change Material Sb_2Se_3 in a Micro-Ring Resonator," *Journal of Physics: Conference Series* 2597, no. 1 (2023): 012020. IOP Publishing.
https://doi.org/10.1088/1742-6596/2597/1/012020

49. S. Zhou, Z. Wang, J. Nong, et al., "Optimized Wideband and Compact Multifunctional Photonic Device Based on Sb_2S_3 Phase Change Material," Optics Express 32, no. 6 (2024): 8506–8519.
https://doi.org/10.1364/OE.507769

50. Kuznetsov, A. I. Miroshnichenko, A. E. Fu, Y. H. Zhang, J. and B. Luk'yanchuk, "Magnetic Light," *Scientific Reports* 2, no. 1 (2012): 492.
https://doi.org/10.1038/srep00492

51. Smirnova, D. and Y. S. Kivshar, "Multipolar Nonlinear Nanophotonics," *Optica* 3, no. 11 (2016): 1241–1255.
https://doi.org/10.1364/OPTICA.3.001241

52. Kuznetsov, A. I. Miroshnichenko, A. E. Brongersma, M. L. Kivshar, Y. S. and B. Luk'yanchuk, "Optically Resonant Dielectric Nanostructures," *Science* 354, no. 6314 (2016): aag2472.
https://doi.org/10.1126/science.aag2472

53. Z. Zheng, D. Smirnova, G. Sanderson, et al., "Broadband Infrared Imaging Governed by Guided-Mode Resonance in Dielectric Metasurfaces," *Light: Science & Applications* 13, no. 1 (2024): 249.
https://doi.org/10.1038/s41377-024-01535-w

54. Z. Zheng, L. Xu, L. Huang, et al., "Boosting Second-Harmonic Generation in the $LiNbO_3$ Metasurface Using High-Q Guided Resonances and Bound States in the Continuum," *Physical Review B* 106, no. 12 (2022): 125411.
https://doi.org/10.1103/PhysRevB.106.125411

55. A. Barreda, C. Zou, A. Sinelnik, et al., "Tuning and Switching Effects of Quasi-BIC States Combining Phase Change Materials with All-Dielectric Metasurfaces," *Optical Materials Express* 12, no. 8 (2022): 3132–3142.
https://doi.org/10.1364/OME.462695

56. Zheng, Z. Xu, L. Huang, L. Smirnova, D. Zangeneh Kamali, K. Yousefi, A. Deng, F. et al., "Third-Harmonic Generation and Imaging with Resonant Si Membrane Metasurface," *Opto-Electronic Advances* 6, no. 8 (2023): 220174.
https://doi.org/10.29026/oea.2023.220174

57. Fan, S. and J. D. Joannopoulos, "Analysis of Guided Resonances in Photonic Crystal Slabs," *Physical Review B* 65, no. 23 (2002): 235112.
https://doi.org/10.1103/PhysRevB.65.235112